J Mater Sci (2009) 44:5569–5578
DOI 10.1007/s10853-009-3781-4

Interfacial study of Crofer 22 APU interconnect-SABS-0 seal glass for solid oxide fuel/electrolyzer cells

M. K. Mahapatra · K. Lu

Received: 19 May 2009 / Accepted: 25 July 2009 / Published online: 8 August 2009

Abstract In planar solid oxide fuel and electrolyzer cells, compatibility and thermochemical stability of interconnect-seal glass interface is essential in order to avoid mixing and leakage of different gases and degradation of cell performances. In the present work, interfacial compatibility and thermochemical stability are studied for an alkaline earth silicate based glass (SABS-0) and Crofer 22 APU interconnect system with respect to thermal treatment temperature (700–850 °C) and time (0–100 h). The study has been carried out in argon to avoid complications from oxidation. Even though pore and crack-free interface is obtained and maintained for all the thermal treatment conditions, there are simultaneous diffusion of the Crofer 22 APU and the SABS-0 glass elements, chemical reaction at the Crofer 22 APU/SABS-0 interface, and devitrification of the SABS-0 glass itself.

Introduction

Planar solid oxide fuel and electrolyzer cells are being actively studied because of their high power density, low cost, and relative ease of fabrication. However, stable and gastight seal is required in order to stack multiple cells without air and fuel mixing and leakage [1, 2]. Extensive work has been carried out to develop glass seals [3, 4]. To be used as a seal, a glass should meet a combination of several requirements. First, the glass seal should have long-term (>5000 h for mobile applications and >40000 h for stationary applications) thermal and chemical stability to withstand severe oxidizing and reducing environments at operating temperatures (700–900 °C). Second, the seal should bond well with other solid oxide fuel/electrolyzer cell components which include electrolyte (stabilized cubic zirconia), interconnect (high chromium ferritic stainless steel), and electrodes (lanthanum strontium manganite and Ni–ZrO_2 cermet) without severe reactions. Third, at the seal-interconnect interface, chromium diffusion from the interconnect into the glass seal should be minimal in order to prevent electrical resistivity decrease and 'chromium poisoning'. Iron from the interconnect side should not diffuse extensively into the glass side since formation and growth of conductive Fe-containing phases may create a short circuit in the cell stack [5]. Diffusion of glass seal elements into the interconnect should also be avoided in order to retain stable glass network structure. Also, inter-diffusion of different species can create new and undesirable interfacial behaviors. Fourth, the thermal expansion coefficient (CTE) of the glass seal should match with those of the interfacing cell components in order to avoid formation of pores or cracks from thermal stress.

Among all the solid fuel/electrolyzer oxide cell components, the interaction of the glass seal with the metallic interconnect is the most crucial. BaO–CaO–Al_2O_3–B_2O_3–SiO_2 based glass has been extensively studied as a seal because of its high CTE ($\sim 11.0 \times 10^{-6}$/K). However, this family of glass reacts with chromium in the interconnect. The reaction product is the detrimental $BaCrO_4$ of very high CTE ($21.0–23.0 \times 10^{-6}$/K). Due to the thermal expansion mismatch between $BaCrO_4$ and the glass seal, thermal stress arises resulting in pores and cracks at the

M. K. Mahapatra · K. Lu (✉)
Department of Materials Science and Engineering,
Virginia Polytechnic Institute and State University,
Blacksburg, VA 24061, USA
e-mail: klu@vt.edu

M. K. Mahapatra
e-mail: mkmanoj@vt.edu

interface [6, 7]. Other BaO–CaO based aluminosilicate systems also react severely with the metal interconnect material and induce cracks at the interface when exposed to either oxidizing or reducing atmosphere [5, 8]. MgO-based aluminosilicate glass reacts severely with the metal interconnect material and forms undesirable cordierite phase of very low CTE (2.0×10^{-6}/K) [9]. Sr–Ca–Y–B–Si based glass systems react with the metal interconnects and form $SrCrO_4$ of high CTE (~ 21.0–23.0×10^{-6}/K) and pores at the interfaces [10, 11]. It has also been demonstrated that undesirable chromate formation is severe at the interconnect-glass seal-air phase boundary. Most recently, pore and crack-free interface was reported for Na_2O–CaO based aluminosilicate seal and Crofer 22 APU alloy [12]. However, this glass system undesirably contains Na_2O, which may decrease the electrical resistivity of the seal due to high mobility of Na^+ [13], increase the evaporation of the glass constituents, and accelerate the glass reaction with the chromium in the interconnect [14].

For most of the interconnect-seal interfacial studies, the experiments have been conducted in an oxidizing atmosphere. A thin chromia layer forms on the interconnect which is believed to increase the bonding ability and inhibit chromium diffusion into the glass seal. However, the chromia layer reacts with the seal glass and causes the formation of undesirable $BaCrO_4$ and $SrCrO_4$. The detrimental chromate formation may be eliminated by avoiding direct exposure of the interconnect-glass seal boundary to air. Glass seal can be bonded with the interconnect in an inert atmosphere, such as argon.

To achieve strong bonding with the metal interconnect, the glass seal and the metal must have certain extent of inter-diffusion, which is dependent on the bonding temperature and time for a given atmosphere. Stability of the interconnect-glass seal interface has been studied as a function of thermal treatment time but no literature report is available regarding the impact of the thermal treatment temperature.

Recently, we developed a SrO–La_2O_3–Al_2O_3–SiO_2 based glass (SABS-0) with almost all the desired thermophysical properties and thermal stability of a solid oxide cell seal glass [15–17]. However, its interfacial compatibility and thermochemical stability with the metallic interconnect have not been studied. This study is focused on these specific issues with Crofer 22 APU as the interconnect alloy. The interfacial study is carried out by microstructure, compositional, and phase analyses using scanning electron microscopy (SEM), energy dispersive spectroscopy (EDS), and X-ray diffraction (XRD). The thermal treatment temperature has been varied from 700 to 850 °C and the thermal treatment time has been changed from 0 to 100 h. Diffusion distance, chemical reaction, and devitrification of the SABS-0 glass at the interface have been analyzed. A multi-event interfacial process has been proposed and discussed.

Experimental procedure

Glass preparation

SABS-0 glass was prepared with conventional glass manufacturing process. Each glass powder batch size was 50 g. $SrCO_3$ (99.9%, Sigma Aldrich, St. Louis, MO), La_2O_3 (99.98%), Al_2O_3 (99.95%), and SiO_2 (99.8%) (all oxides were from Alfa Aesar, Ward Hill, MA) at designed ratios were mixed in a ball mill for overnight. The mixed powders were heated in a platinum crucible in a box furnace (Lindberg, Model No. 51314, Watertown, WI) to 1100 °C and kept there for 1 h for $SrCO_3$ to decompose. After that, the mixture was heated to 1400 °C for 4 h. The heating rate was 10 °C min^{-1}. The molten glass was quenched into a graphite mold.

Sample preparation for interfacial study

Crofer 22 APU samples (ThyssenKrupp VDM, Germany) were polished to optical finish using polishing papers followed by 1 μm Al_2O_3 particle suspension and 0.05 μm SiO_2 sol to remove oxidized layer, if any, and to obtain scratch-free flat surface. The composition of the Crofer 22 APU is given in Table 1 [6]. The polished samples were cleaned by ultrasound in water and then in acetone before being dried and wiped with acetone. A clean and flat SABS-0 glass piece was put on the polished Crofer 22 APU surface and thermally treated at 960 °C for 30 min in argon in order to bond the SABS-0 glass with the Crofer 22 APU. No external pressure was applied during the bonding process.

The bonded Crofer 22 APU/SABS-0 sample was thermally treated at 700, 750, 800, and 850 °C for 100 h in argon atmosphere. In addition, the thermal treatment at 800 °C was carried out for different times (0–100 h). First, the bonded Crofer 22 APU/SABS-0 sample was thermally treated for 10 h. Then, a portion of the Crofer 22 APU/SABS-0 sample was removed. The remaining part of the Crofer 22 APU/SABS-0 sample was thermally treated for 20, 50, and 100 h, respectively. The dwell times at 800 °C were accumulative with interruptions for sample removal. The same heating and cooling rates of 3 °C min^{-1} were used for all the thermal treatment experiments.

Table 1 Crofer 22 APU alloy composition (wt%) (ThyssenKrupp VDM, Germany) [6]

Cr	Fe	Mn	Ti	Si	Al	C	S	P	Re
22.8	Balance	0.45	0.08	–	–	0.005	0.002	0.016	0.06 La

Characterization

The cross sections of all the thermally treated diffusion couples were finely polished to optical finish. Field emission SEM (Quanta 600 FEG, FEI Company, Hillsboro) was used to examine the interfacial morphology between the SABS-0 glass and the Crofer 22 APU interconnect under secondary electron mode. The EDS module (Bruker AXS, MiKroanalysis, Gmbh, Berlin, Germany) attached to the SEM was used for composition analysis in order to understand the elemental distribution in the Crofer 22 APU metal and the SABS-0 glass. The analyses followed standard procedures in the field. The elemental distribution along the interface was determined by EDS line scan and area mapping. For all the studied samples, the EDS line scan was done in at least three randomly selected regions. The results given here are the averages of these scan data. The beam current was kept at 224 μA for all the analyses. The accelerating voltage was 10 kV for the SEM mode and 15 kV for the EDS spectra. The working distance was 11.0–11.7 mm for the SEM mode and 10.0 mm for the EDS spectra.

To investigate the devitrified phases at the interface of the Crofer 22 APU/SABS-0 couple, high-resolution XRD studies were carried out in an X'Pert PRO diffractometer (PANalytical B.V., EA Almelo, The Netherlands). SABS-0 glass coated Crofer 22 APU surface was polished until the glass layer was 15–20 μm thick. Such SABS-0 glass layer thickness was deemed suitable since X-ray detects 95% of the phase information from 25 μm penetration depth [18]. The scan time per step was 3000 s with CuK_{α} radiation ($\lambda = 1.5406$ Å). The XRD voltage was 45 kV and the beam current was 40 mA.

Results and discussion

The thermophysical properties of the SABS-0 glass have been discussed elsewhere [16] and can be summarized as follows. The glass transition temperature (the start of T_g) is 775 ± 2.75 °C, the dilatometric softening point (T_d) is 815 °C, and the CTE is $10.8 \pm 0.5 \times 10^{-6}$/K over 50–775 °C temperature range, which matches closely with that of the Crofer 22 APU alloy ($11.4–12.5 \times 10^{-6}$/K) [19–21]. No crystalline phase is observed after 200 h of thermal treatment at 850 °C in air.

Crofer 22 APU/SABS-0 glass interfacial microstructure

The microstructures of the Crofer 22 APU/SABS-0 couple thermally treated at 700, 750, 800, and 850 °C in argon for 100 h are given in Fig. 1. The microstructures at different temperatures show distinct, intimate, and pore-free

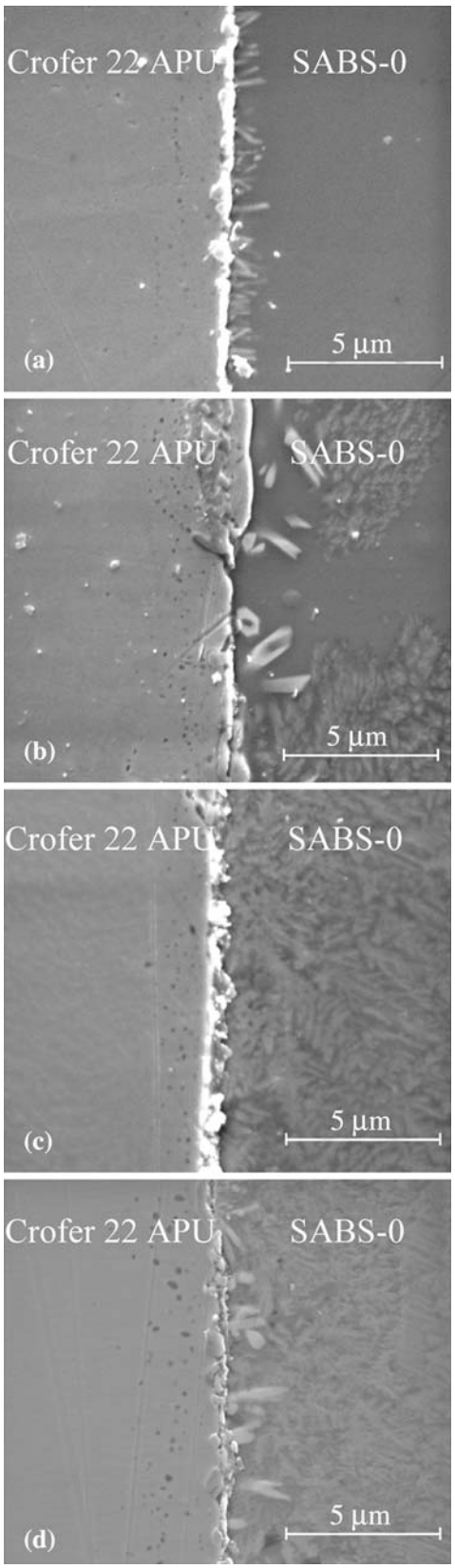

Fig. 1 SEM images of the Crofer 22 APU/SABS-0 samples thermally treated at different temperatures for 100 h: **a** 700 °C, **b** 750 °C, **c** 800 °C, and **d** 850 °C

interfaces. The interfacial zone thickness fluctuates but is generally less than 3 μm. Elongated phases with different orientations can be seen in the SABS-0 glass matrix close to the interface. The elongated phases are only present in the regions very close to the interface for the thermally treated sample at 700 °C. For the 750 °C thermally treated sample, the elongated phases are locally distributed in the SABS-0 glass matrix. However, for the 800 and 850 °C thermal treatment conditions, the elongated phases extend well into the SABS-0 glass matrix. This means the amount of the elongated phases increases with thermal treatment temperature. Based on our prior work on similar glass compositions, the elongated phases are the newly devitrified phases [22, 23]. This is also consistent with the knowledge that localized devitrification can occur when a glass is bonded to metal [24]. However, the elongated phases in the SABS-0 glass do not exist beyond 10 μm on the SABS-0 glass side (lower magnification images are not shown) and show little impact on the interfacial bonding quality. For all the Crofer 22 APU/SABS-0 samples treated at different temperatures, small black spots ($\ll$1 μm) can be seen on the interconnect side near the interface. These are closed pores which form as a result of chromium evaporation from the interconnect [25]. At the studied temperatures the pore sizes are $\ll$1 μm.

The microstructures of the Crofer 22 APU/SABS-0 samples thermally treated at 800 °C for different dwell times are given in Fig. 2. The SABS-0 glass bonds well with the Crofer 22 APU alloy as seen in Fig. 2a. In the as-bonded sample (Fig. 2a), elongated, needle-shaped bright phase on the SABS-0 glass side is observed. For all the thermally treated samples, such elongated phases become more widespread on the SABS-0 glass side. The samples show a distinct, thin interfacial layer. Evolution of the interfacial layer with thermal treatment time suggests that the diffusion of the Crofer 22 APU and the SABS-0 glass elements plays an important role in the interfacial new phase formation. Again, small pores ($\ll$1 μm) near the interface on the Crofer 22 APU side are observed, similar to the samples thermally treated for 100 h at different temperatures. While such small, closed pores are not a problem at such short thermal treatment times, it should be closely monitored for long-term solid oxide fuel/electrolyzer cell operation conditions.

Elemental distribution across the Crofer 22 APU/SABS-0 interface

Elemental distribution across the interface of the Crofer 22 APU/SABS-0 samples thermally treated at different temperatures for 100 h is given in Fig. 3. On the x-axis, '0' indicates the center of the interface. The left (negative) side is the Crofer 22 APU alloy and the right (positive) side is

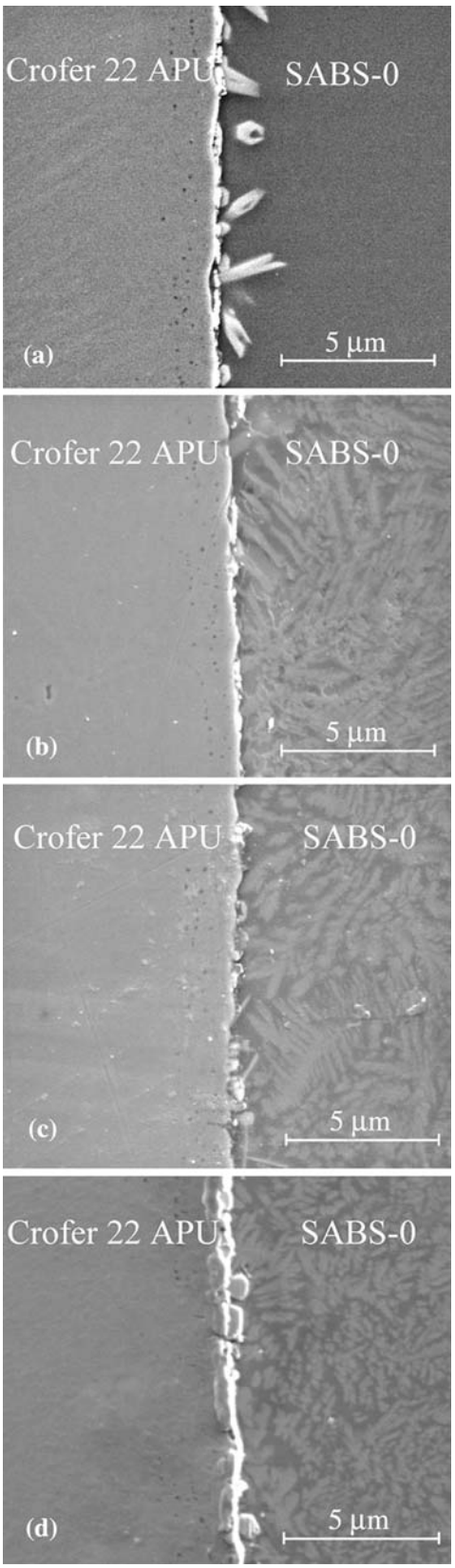

Fig. 2 SEM images of the Crofer 22 APU/SABS-0 samples thermally treated at 800 °C for different times: **a** as-bonded, **b** 10 h, **c** 20 h, and **d** 50 h

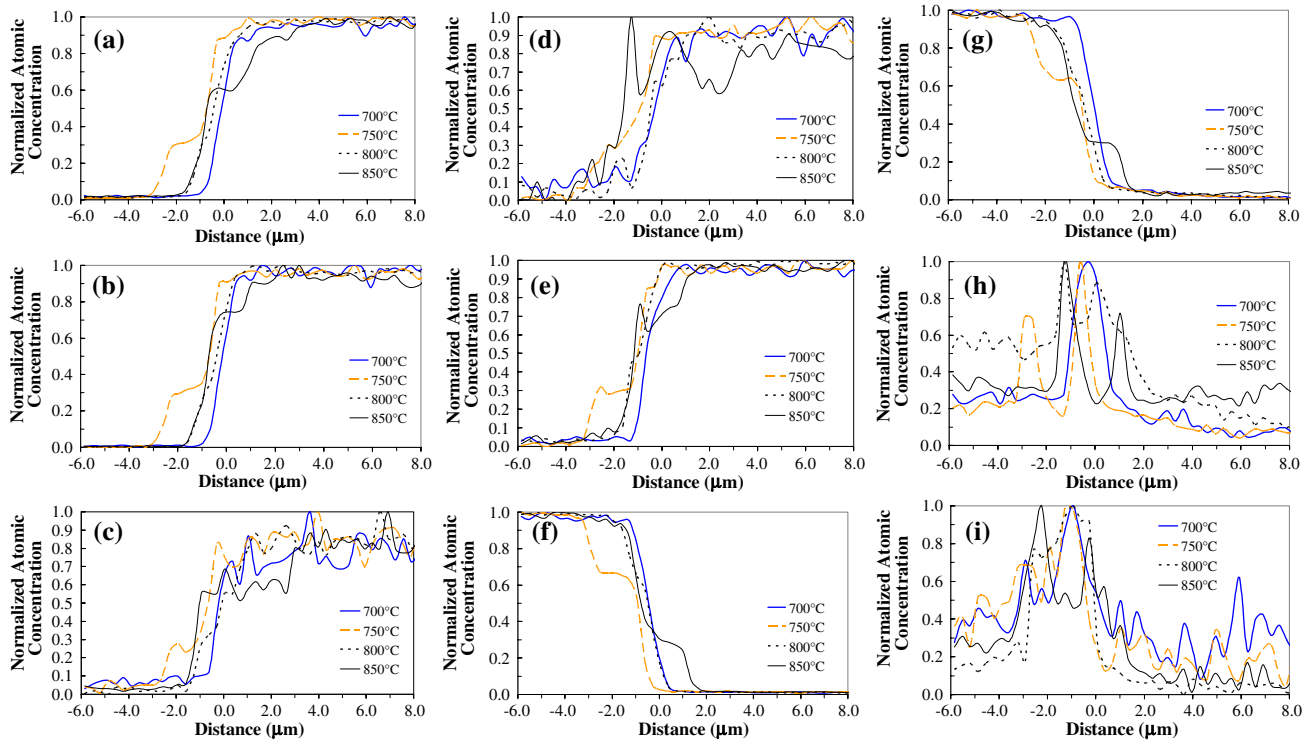

Fig. 3 Elemental distribution of the Crofer 22 APU/SABS-0 samples thermally treated at different temperatures for 100 h: **a** Si, **b** Sr, **c** La, **d** Al, **e** O, **f** Fe, **g** Cr, **h** Mn, and **i** Ti

the SABS-0 glass. The atomic concentration of each element has been normalized based on its maximum concentration as shown on the *y*-axis. From the microstructures in Figs. 1 and 2, it can be seen that diffusion and chemical reaction occur between the SABS-0 glass and the Crofer 22 APU alloy. Devitrification of the SABS-0 glass is also observed. Chemical reaction between the Crofer 22 APU alloy and the SABS-0 glass and devitrification of the SABS-0 glass itself make quantitative diffusion analysis ambiguous. The elemental distribution profile across the interface is not the classical 'S' shape. Still, approximate diffusion distance can be determined by identifying the inflection point and diffusion tail at the interface. All the elements in the SABS-0 glass, silicon, strontium, lanthanum, aluminium, and oxygen, diffuse 2–3 μm into the Crofer 22 APU alloy side. Iron in the Crofer 22 APU alloy diffuses 2–3 μm into the SABS-0 glass. Chromium diffuses ~5 μm into the SABS-0 glass for the samples thermally treated at 700 and 750 °C and ~7 μm into the SABS-0 glass for the samples thermally treated at 800 and 850 °C. The concentrations of manganese and titanium are at maximum at the interface as revealed from the sharp peaks at the interface. Also, titanium concentration peaks shift to the left in comparison to the manganese peaks. Manganese (0.45 wt%) and titanium (0.08 wt%) are the minor elements in the Crofer 22 APU alloy. Manganese is added in the Crofer 22 APU alloy to suppress chromium evaporation and diffusion. Titanium is added to improve the electrical conductivity of the alloy [26]. Since manganese and titanium have higher affinity with oxygen than chromium [27, 28], they are more likely to react with oxygen and form oxides to prevent further Crofer 22 APU alloy degradation [29, 30]. Because of their higher oxygen affinity and diffusivity, manganese and titanium accumulate at the interface and hinder the diffusion of the SABS-0 glass elements and the Crofer 22 APU elements into each other.

Below 800 °C, the thermal treatment temperature does not have a clear impact on the elemental distribution profile. As the thermal treatment temperature increases from 800 to 850 °C, the elemental distribution profiles become more irregular.

Elemental distribution of the Crofer 22 APU/SABS-0 sample thermally treated at 800 °C for different thermal treatment times is shown in Fig. 4. The elements in the SABS-0 glass and iron in the Crofer 22 APU alloy diffuse a similar distance of ~2 μm. This implies that the diffusion of the SABS-0 glass elements is not significantly affected by the thermal treatment time for up to 100 h. Chromium in the Crofer 22 APU alloy diffuses into the SABS-0 glass at ~5 μm in the as-bonded sample. The diffusion distance of chromium increases to ~7 μm in the 50 h thermally treated sample and remains almost unchanged for the 100 h thermally treated sample. This suggests that chromium diffusion increases with the thermal treatment time.

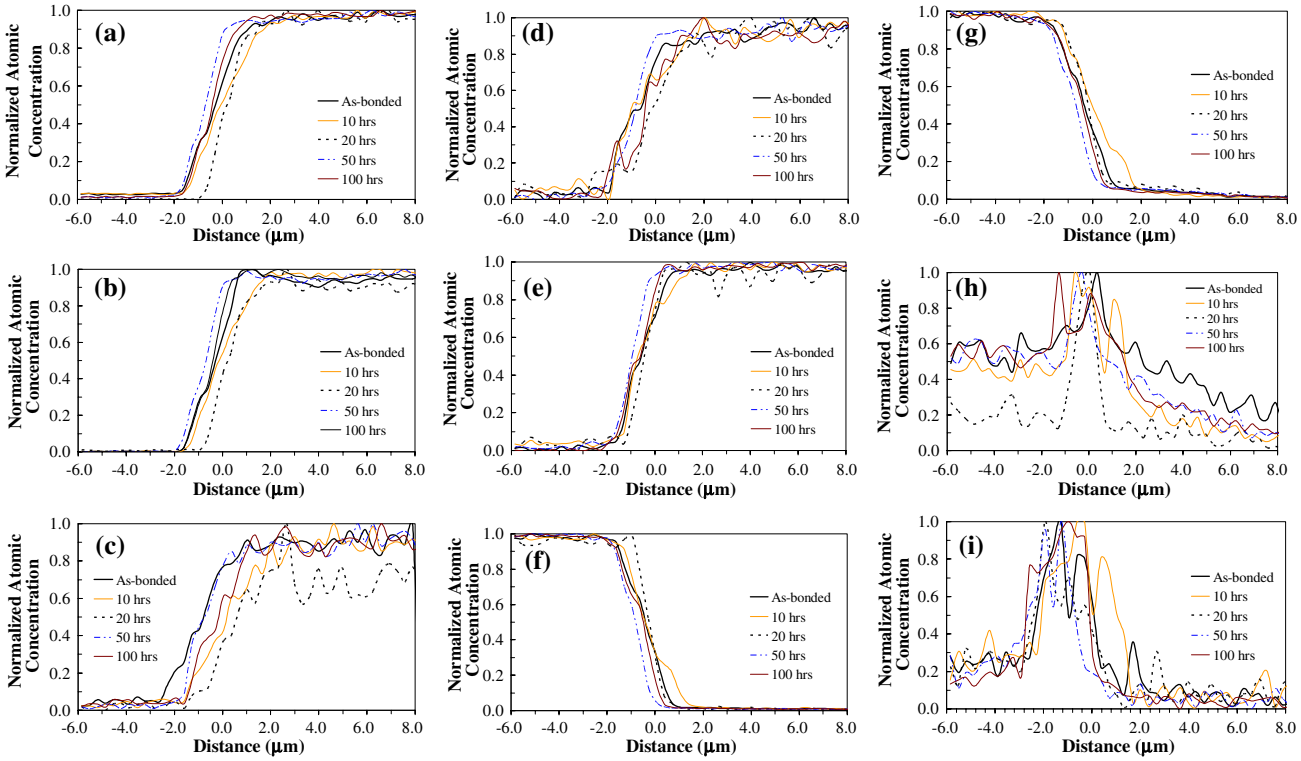

Fig. 4 Elemental distribution of the Crofer 22 APU/SABS-0 samples thermally treated for different times at 800 °C: **a** Si, **b** Sr, **c** La, **d** Al, **e** O, **f** Fe, **g** Cr, **h** Mn, and **i** Ti

Manganese and titanium concentrations are highest at the interface. Again, titanium peaks reside beneath the manganese-rich layer on the Crofer 22 APU side.

The diffusion distances of the SABS-0 glass elements and the Crofer 22 APU elements except for chromium remain unchanged at ~2 μm with different thermal treatment time. Such diffusion distances are close to the interfacial zone thickness (<3 μm) shown in Figs. 1 and 2. This indicates that the interface is formed by the diffusion-controlled chemical reaction. The fluctuations in lanthanum and aluminium distributions may be due to the compositional difference between the elongated crystalline phases and the glass matrix. Diffusion distance of chromium also remains unchanged at ~7 μm after 50 h of thermal treatment time. Longer diffusion distance of chromium than that of other elements in the Crofer 22 APU alloy suggests that volatile chromium species might have diffused into the SABS-0 glass.

To further understand the interaction between the Crofer 22 APU alloy and the SABS-0 glass at the interface, elemental mapping results are shown in Fig. 5 for the sample thermally treated at 850 °C for 100 h. This thermal treatment condition should provide the most severe interfacial interaction scenario. As shown, the interfacial layer has higher concentrations of manganese and titanium from the Crofer 22 APU alloy and lanthanum and oxygen from the SABS-0 glass. Consistent with the EDS plot (Fig. 3h, i), titanium-enriched layer is present beneath the manganese-enriched layer. Chromium is also rich at localized interfacial spots. Aluminium and lanthanum have also diffused to the Crofer 22 APU side. Other than the above observations, the distributions of both the Crofer 22 APU and the SABS-0 glass elements are homogeneous after thermal treatment at 850 °C for 100 h. This means the elongated phases on the SABS-0 glass side observed in Figs. 1 and 2 are due to the devitrification of the SABS-0 glass.

X-ray diffraction analysis

In addition to the microstructure and the elemental distribution results obtained, the Crofer 22 APU/SABS-0 glass interfacial phase changes need to be understood. From sections "Crofer 22 APU/SABS-0 glass interfacial microstructure" and "Elemental distribution across the Crofer 22 APU/SABS-0 interface" it cannot be determined what the elongated phases are on the SABS-0 glass side. XRD analysis of the Crofer 22 APU/SABS-0 interface can address this issue. In this study, the SABS-0 glass layer is thin enough that all the phases at the interface can be detected by passing X-ray from the top of the SABS-0 glass layer into the Crofer 22 APU alloy.

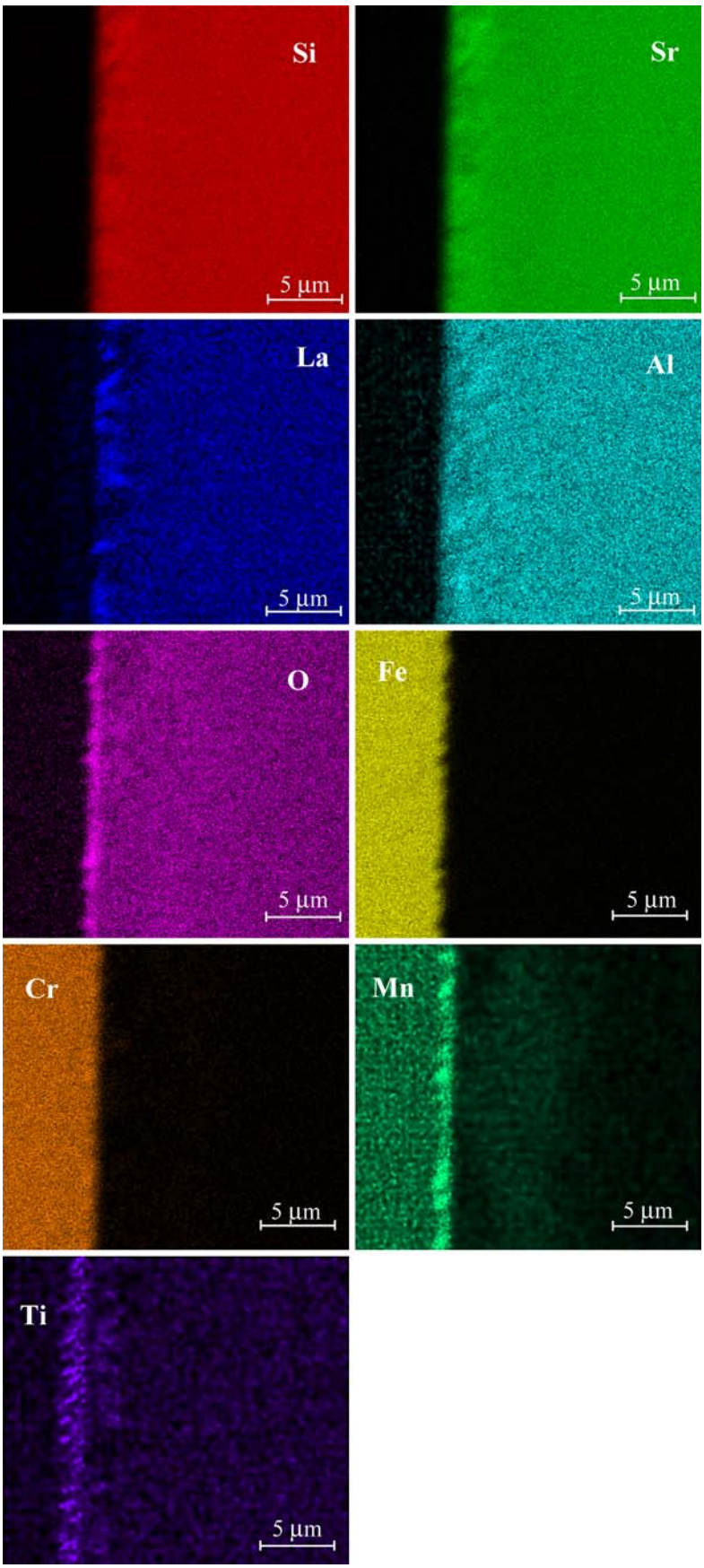

Fig. 5 Elemental distribution maps of the Crofer 22 APU/SABS-0 sample thermally treated at 850 °C for 100 h

The XRD pattern of bulk SABS-0 glass at as-bonded condition is shown in Fig. 6a. XRD pattern of amorphous SABS-0 glass can be observed. The XRD pattern for the Crofer 22 APU alloy is shown in Fig. 6b. The characteristic (110) peak of iron at 44.67° (JCPDS No. 87-0721) can be seen. The XRD patterns for the as-bonded Crofer 22 APU/SABS-0 sample and the thermally treated Crofer 22 APU/SABS-0 at different temperatures for 100 h are given in Fig. 7. The presence of the characteristic (110) peak of iron at 44.67° in all the samples confirms that the XRD patterns include all the crystal phases across the interface. For the bonded samples, the indexing of X-ray patterns was done using standard method for polycrystalline materials [31]. First, the highest intensity peaks are matched with all the combinations of compounds consisting of the Crofer 22 APU alloy and the SABS-0 glass elements. The difference between the *d*-spacing of the experimental results and the standard (JCPDS) should be less than 0.04 Å. Then, the highest number of the matched peaks with the lowest possible *d*-spacing difference is considered. As Fig. 7 shows, new crystalline phases are present at the Crofer 22 APU/SABS-0 interfaces for all the samples. The crystal phases can be identified as monoclinic $La_2Cr_2O_9$ (JCPDS No. 49-1571) and hexagonal $Sr_7Al_{12}O_{25}$ (JCPDS No. 83-2325). It should be noticed that the peaks of these two phases overlap. By comparing the intensity ratio of the experimental result with the standard data, $La_2Cr_2O_9$ phase is the major phase and $Sr_7Al_{12}O_{25}$ is the minor phase. So, the peaks in Fig. 7 are indexed for $La_2Cr_2O_9$. The same number and location of peaks in the XRD patterns mean that the crystal phases are the same for all the studied thermal treatment times and temperatures. However, the XRD peak intensities vary. This is likely due to the thermal treatment effect and the slightly different thickness of the SABS-0 glass layer on the Crofer 22 APU alloy. It is very challenging to obtain the same SABS-0 glass layer thickness and this effect has not been de-convoluted.

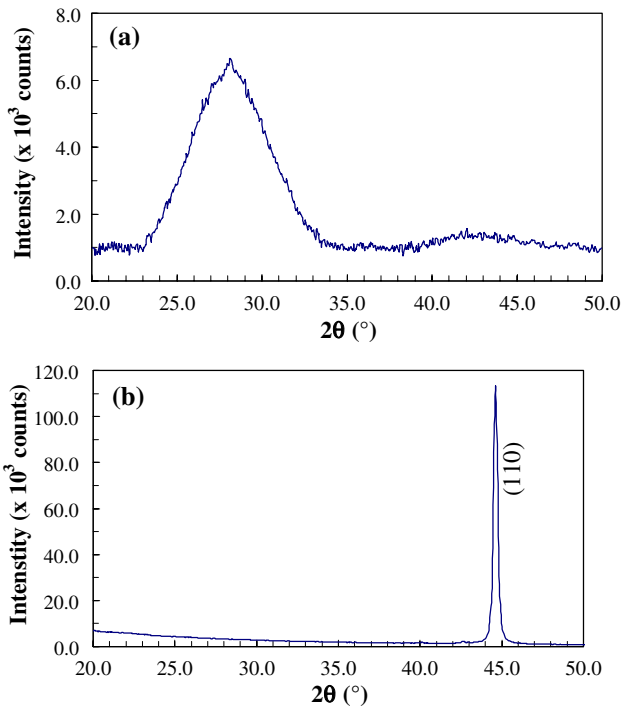

Fig. 6 XRD patterns of **a** SABS-0 glass thermally treated at 960 °C for 30 min and **b** Crofer 22 APU alloy

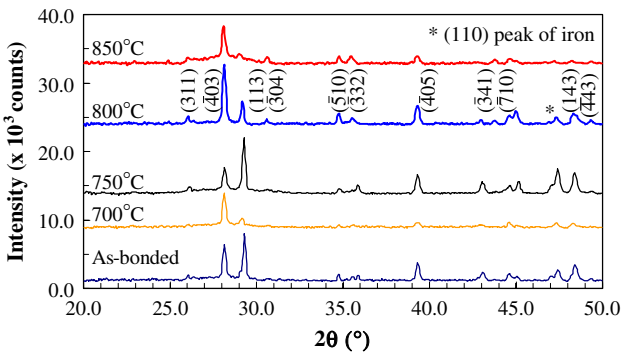

Fig. 7 XRD patterns at the Crofer 22 APU/SABS-0 interfaces. The samples include the as-bonded condition and the thermally treated conditions at different temperatures for 100 h

Based on the identification of the crystalline phases, it can be understood that devitrification occurs in the SABS-0 glass itself and causes formation of $Sr_7Al_{12}O_{25}$. The process can be understood as follows. In the SABS-0 glass, Al^{3+} is a glass former [15]; Sr^{2+} is a charge compensator for the nearest localized $(AlO_4)^-$ tetrahedral structural units [32]. Microheterogeneity in the SABS-0 glass structure, such as localized $(AlO_4)^-$ tetrahedral units, induces the devitrification of the SABS-0 glass. Accordingly, $Sr_7Al_{12}O_{25}$ crystalline phase forms.

As to the formation of $La_2Cr_2O_9$, the process can be understood as follows. La_2O_3 containing glass tends to form energetically favorable, isolated, small, and phase ordered clusters. These clusters generally contain La–O–La structural units. In our previous work [16], these La–O–La structural units are overlapped in 1105 and 1010 cm^{-1} wave numbers in the Raman spectra of the SABS-0 glass. These isolated La–O–La clusters act as nucleation sites for devitrification of the SABS-0 glass [33, 34]. The elemental mapping results in Fig. 5 show accumulation of lanthanum and oxygen at the interface. At the same time, chromium diffuses to the SABS-0 glass side as observed from the EDS analysis (Figs. 3g and 4g). This leads to the breakdown of the SABS-0 glass network structure [35]. According to Sanderson, acidobasicity value, a glass property related to the chemical environment, is 3.50 for chromium and 1.95 for lanthanum [36]. This means

chromium is acidic and lanthanum is basic in nature. Therefore, reaction among lanthanum, chromium, and oxygen favors $La_2Cr_2O_9$ formation. From a different aspect, chromium evaporation from the Crofer 22 APU alloy occurs based on the presence of closed pores near the interface (Figs. 1 and 2). So $La_2Cr_2O_9$ may form by the reaction:

$$La_2O_3 + 2Cr + 6O_{glass} = La_2Cr_2O_9$$

If residual H_2O in glass is considered, $CrO_2(OH)_2$ is the thermodynamically favorable and dominant vapor species compared to CrO_2OH [7, 37, 38] and CrO_3 (oxidizing atmosphere) [39]. In this case, the formation of $La_2Cr_2O_9$ follows the reactions:

$$La_2O_3 + 2CrO_2(OH)_2(g) = La_2Cr_2O_9 + 2H_2O(g)$$

Elemental mapping results in Fig. 5 show that lanthanum accumulates at the interface. So, $La_2Cr_2O_9$ phase, likely a result of diffusion-controlled reaction, should be the interfacial crystalline phase. The presence of the $Sr_7Al_{12}O_{25}$ crystal phase in the XRD patterns is due to the devitrification of the SABS-0 glass (Fig. 7). This means that the devitrification of the SABS-0 glass and the chemical reaction of the SABS-0 glass with the Crofer 22 APU alloy occur simultaneously along with the diffusion of the Crofer 22 APU/SABS-0 elements.

Multi-event process at the interface

From the microstructure, the EDS line scan and area mapping, and the XRD results, it can be determined that at least three processes, diffusion, chemical reaction, and devitrification of the SABS-0 glass, occur during the thermal treatment of the Crofer 22 APU/SABS-0 samples. Chromium diffuses 5–7 μm into the SABS-0 glass. $La_2Cr_2O_9$ is the reaction product as discussed in section "X-ray diffraction analysis". Therefore, the chemical reaction at the interface is controlled by the diffusion process since diffusion must occur prior to the chemical reaction. After the chemical reaction, strong bonding at the metal-glass interface forms. However, the diffusion of the Crofer 22 APU elements into the SABS-0 glass breaks the SABS-0 glass network structure and enhances the devitrification of the SABS-0 glass. This is further supported by the comparable distances of chromium diffusion into the SABS-0 glass (5–7 μm) and the devitrified glass phases near the interface (less than ~10 μm). However, the diffusion process is complicated by the presence of multiple components in the SABS-0 glass and the Crofer 22 APU alloy, the chemical reaction, and the devitrication of the SABS-0 glass. If the diffusion of chromium can be eliminated, then the chemical reaction and the break-down of the SABS-0 glass network can be avoided. So, the fundamental cause of the interfacial degradation can be attributed to the chromium diffusion induced chemical reaction and devitrification.

Previous efforts regarding the interconnect-seal glass interaction [5–12] are mainly based on microstructure and EDS spot analysis. These studies only address the chemical reaction(s) at the interface and the diffusion of the interconnect alloy and the glass seal elements. EDS, however, cannot detect specific compound species or crystalline phases. The devitrification of seal glass or glass-ceramic has been observed but not been addressed from the interfacial phase formation point of view. Cr_2O_3, $BaCrO_4$, and $SrCrO_4$ have been claimed as the reaction products only by comparing the EDS spot analysis results with theoretical thermodynamics without considering reaction kinetics. The $(Mn,Cr)_3O_4$ spinel layer formed at the Crofer 22 APU interface is assumed to be the active barrier layer for diffusion of both the glass and the Crofer 22 APU elements. However, Cr_2O_3 and $(Mn,Cr)_3O_4$ spinel are not observed in the XRD pattern in the present study. Little XRD work has been conducted to identify the reaction products as well as the crystalline phases of devitrified glass. A study on glass powders or glass-metal powder mixtures [9] cannot provide insight into the chemical reaction phenomena at the interconnect/seal glass interface.

Almost constant diffusion distances of ~2 μm for all the elements except for chromium at different thermal treatment temperatures and times are observed. Chromium diffusion distance increases from 5 to 7 μm with thermal treatment time and temperature and remains almost unchanged after 100 h of dwell time at 800 and 850 °C. This result indicates that the interfacial interactions may have reached equilibrium after certain thermal treatment time and temperature. Further reaction between the Crofer 22 APU alloy and the SABS-0 glass will not occur once the interface becomes chemically stable [40]. Constant diffusion distance, pore and crack free interface (Figs. 1 and 2), and identical crystalline phases at different thermal treatment time and temperature suggest that the SABS-0 glass is compatible with the Crofer 22 APU interconnect alloy. The devitrified phases are limited and seem to have close CTEs to that of both the SABS-0 glass and the Crofer 22 APU interconnect. Generally, a glass seal of a few hundred microns thick is applied in planar solid oxide cells. Diffusion distance of 7 μm for chromium and 2 μm for the remaining elements should not be a problem. The SABS-0 glass is a promising seal based on the results so far. However, long-term thermal treatment of the Crofer 22 APU alloy/SABS-0 sample in simulated solid oxide fuel/electrolyzer cell operating conditions (air and wet hydrogen atmospheres at 800 °C) needs to be carried out to verify this prediction.

Conclusions

The interfacial compatibility of a $SrO–La_2O_3–Al_2O_3–SiO_2$ based glass (SABS-0) with Crofer 22 APU interconnect material has been investigated for different thermal treatment temperatures (700–850 °C) and times (0–100 h). Diffusion-controlled chemical reaction at the interface and the devitrification of the SABS-0 glass itself are observed. Diffusion of the SABS-0 glass and the Crofer 22 APU alloy elements occurs prior to the chemical reaction at the interface. Chromium in the Crofer 22 APU alloy participates in the chemical reaction with the SABS-0 glass and $La_2Cr_2O_9$ forms at the interface. Chromium diffusion facilitates SABS-0 glass devitrification and $Sr_7Al_{12}O_{25}$ crystal phase formation in the glass matrix. The SABS-0 glass is compatible with the Crofer 22 APU interconnect under the studied conditions but longer term validation is needed.

Acknowledgements This material is based on work supported by Department of Energy under Award Number DE-FC07-06ID14739. The SEM analysis was done in Nanoscale Characterization and Fabrication Laboratory (NCFL), Virginia Tech. The authors are indebted to Dr. Zhenguo "Gary" Yang, Pacific Northwest National Laboratory, Richland, Washington, for providing Crofer 22 APU alloy for this study.

References

1. EG & G Technical Services (2004) Fuel cell handbook, 7th edn. US Department of Energy, Office of Fossil Energy, National Energy Technological Laboratory, pp 7–12
2. Singhal SC, Kendall K (2003) High temperature solid oxide fuel cells. Elsevier, Oxford, p 217
3. Lessing PA (2007) J Mater Sci 42:3465. doi:10.1007/s10853-006-0409-9
4. Fergus JW (2005) J Power Sources 147:46
5. Batfalsky P, Haanappel VAC, Malzbender J, Menzler NH, Shemet V, Vinke IC, Steinbrech RW (2006) J Power Sources 155:128
6. Yang Z, Xia G, Meinhardt KD, Weil KS, Stevenson JW (2004) J Mater Eng Perform 13:327
7. Yang Z, Meinhardt KD, Stevenson JW (2003) J Electrochem Soc 150:A1095
8. Haanappel VAC, Shemet V, Vinke IC, Gross SM, Koppitz TH, Menzler NH, Zahid M, Quadakkers WJ (2005) J Mater Sci 40:1583. doi:10.1007/s10853-005-0657-0
9. Lahl N, Bahadur D, Singh K, Singheiser L, Hilpert K (2002) J Electrochem Soc 149:A607
10. Chou YS, Stevenson JW, Singh P (2007) J Electrochem Soc 154:B644
11. Chou YS, Stevenson JW, Gow RN (2007) J Power Sources 170:395
12. Smeacetto F, Salvo M, Ferraris M, Cho J, Boccaccini AR (2008) J Eur Ceram Soc 28:61
13. Melling PJ, Vempati CJ, Allmatt AR, Jacobs PWM (1981) Phys Chem Glasses 22:49
14. Ogasawara K, Kameda H, Matsuzaki Y, Sakurai T, Uehara T, Toji A, Sakai N, Yamaji K, Horita T, Yokokawa H (2007) J Electrochem Soc 154:B657
15. Lu K, Mahapatra MK (2008) J Appl Phys 104:074910
16. Mahapatra MK, Lu K, Bodnar RJ (2009) Appl Phys A 95:493
17. Mahapatra MK, Lu K (2008) J Power Sources 185:993
18. Cullity BD (1978) Elements of X-ray diffraction, 2nd edn. Addison-Wesley Publishing Company Inc., Philippines, pp 292–294
19. Smeacetto F, Salvo M, Ferraris M, Casalegno V, Asinari P, Chrysanthou A (2008) J Eur Ceram Soc 28:2521
20. Lara C, Pascual MJ, Durán A (2007) Phys Chem Glasses Eur J Glass Sci Tech B 48:218
21. Konysheva E, Laatsch J, Wessel E, Tietz F, Christiansen N, Singheiser L, Hilpert K (2006) Solid State Ionics 177:923
22. Mahapatra MK, Story C, Lu K, Reynolds WT Jr (2007) Energy: fuel cells: materials, processing, manufacturing and power management technologies. In: Proceedings of materials science and technology, Detroit, MI, USA, September 16–20, pp 371–380. Organizers: Singh P, Azad, Collins DC, Kumta PN, Legzdins C, Manthiram A, Manivannan A, Sundaram SK, Yang ZG
23. Mahapatra MK, Lu K, Reynolds WT Jr (2008) J Power Sources 179:106
24. Kumar P, Greenhut VA (1990) Metal-ceramic joining. TMS Minerals, Metals, Materials, Warrendale, PA, pp 3–11
25. Yang Z, Xia G, Wang CM, Nie Z, Templeton J, Stevenson JW, Singh P (2008) J Power Sources 183:660
26. Quadadakkers WJ, Shemet V, Singheiser L (2003) US Patent 0,059,335
27. Beranger G, Armanet F, Lambertin M (1989) In: Lang E (ed) The role of active elements in the oxidation behavior of high temperature metals and alloys. Elsevier Science Publishing Co. Inc., New York, pp 33–51
28. Bennet MJ, Moon DP (1989) In: Lang E (ed) The role of active elements in the oxidation behavior of high temperature metals and alloys. Elsevier Science Publishing Co. Inc., New York, pp 111–129
29. Lobnig RE, Schmidt HP, Hennesen K, Grabke HJ (1992) Oxid Met 37:81
30. Cox MGC, McEnaney B, Scott VD (1972) Philos Mag 2:839
31. Klug HP, Alexander LE (1974) X-ray diffraction procedures for polycrystalline and amorphous materials, 2nd edn. Wiley, New York
32. Cromier L, Calas G, Creux S, Gaskell PH, Bouchet-Fabre B, Hannon AC (1999) Phys Rev B 59:13517
33. Schaller T, Stebbins JF, Wilding MC (1999) J Non-Cryst Solids 243:146
34. Wilding MC, Navrotsky A (2000) J Non-Cryst Solids 265:238
35. Jiang N, Silox J (2000) J Appl Phys 87:3768
36. Volf MB (1984) Chemical approaches to glass: glass science and technology, vol 7. Elsevier, Amsterdam, pp 83–88
37. Kim YW, Belton GR (1974) Metal Trans 5:1811
38. Ebbinghaus BB (1993) Combust Flame 93:119
39. Caplan D, Cohen M (1961) J Electrochem Soc 108:438
40. Pask JA (1987) In: Moddeman WE, Merten CW, Kramer DP (eds) Technology of glass,ceramic or glass-ceramic to metal sealing. The American Society of Mechanical Engineers, New York, pp 1–7